Journal of Hydrology: Regional Studies 48 (2023) 101467

Contents lists available at ScienceDirect

Journal of Hydrology: Regional Studies

journal homepage: www.elsevier.com/locate/ejrh

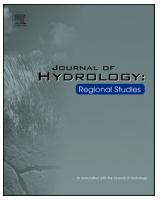

Historical comparison of the damage caused by the propagation of a dam break wave in a pre-alpine valley

Riccardo Bonomelli [a], Gabriele Farina [a], Marco Pilotti [a,*], Daniela Molinari [b], Francesco Ballio [b]

[a] DICATAM, Università degli Studi di Brescia, Brescia, Italy
[b] DICA, Politecnico di Milano, Milano, Italy

ARTICLE INFO

Keywords:
Dam break wave propagation
Shallow water equations
Flood vulnerability and damage

ABSTRACT

Study region: Valle Camonica basin and Lake Iseo in the Italian pre-alpine and alpine region.
Study focus: This paper provides the first hydraulic reconstruction of the terminal part of the Gleno dam break with the propagation of the flood wave along a wide pre-alpine valley. The reconstruction of this part of the event, accomplished with a new 2D Shallow Water Equations solver, provides the occasion to tackle some important issues related to the computation of flood damage, a topic of paramount practical importance for which there is no widely accepted procedure in the literature.
New hydrological insights for the region: The hydraulic reconstruction provides insights into the propagation of the flood through the floodplain as far as the inlet of Lake Iseo. A methodology for damage computation is presented that considers a physically based criterion for the vulnerability of human life, with significant implications with respect to the use of simpler approaches based only on the density of the population. The economic evaluation of the damage to the built environment and to agricultural activities is included through a comprehensive recent approach. We discuss the variations of the expected damage due to the hydraulic works accomplished over the last 100 years to decrease the flood hazard, showing that its reduction has been followed by an increase in the expected damage in the surrounding areas.

1. Introduction

Floods are unavoidable phenomena whose impact on human activities is increasing synergistically with climate change effects and growing level of land anthropization. The increasing exposure of people and economic activities to floods is a mixed consequence of unawareness and necessity. In situations where floods are relatively rare, there is often a wrong sense of safety that is connected to a lack of historical memory. More frequently, the only inhabitable zones are flood-prone areas. In many other situations, although theoretically possible, relocation, that would be the most rational choice, is non-viable due to social, political, and short-term economic costs. Finally, in more limited but important cases, floods can be an unintended consequence of accidents to hydraulic structures present in an otherwise safe territory, as in potentially catastrophic dam-break or dam-breach events in mountain areas. In all these situations the evaluation of the damage caused by floods has a fundamental role to play, with huge economic and social implications. *A priori* damage quantification leads to the prevention, protection, and preparedness against flood adverse consequences for human

* Corresponding author.
E-mail address: marco.pilotti@unibs.it (M. Pilotti).

https://doi.org/10.1016/j.ejrh.2023.101467
Received 7 March 2023; Received in revised form 30 June 2023; Accepted 6 July 2023
Available online 19 July 2023

life, cultural heritage, economic activities, infrastructures and the environment. Accordingly, most international legislations on flood risk management require a change in paradigm: from hazard oriented analyses and mitigation solutions to integrated analyses and strategies, aiming at reducing the risk, i.e. the expected damage. For instance, EU "Floods" Directive 2007/60/EC dictates to update every 6 years flood hazard and risk mapping in correspondence of low, medium, and high probability flood events, as a basis for the development of Flood Risk Management Plans. After the occurrence of an event, *ex post* damage assessment supports the identification of priorities of intervention and the damage compensation process. Whereas there is widespread agreement on the procedure to compute hazard maps through the use of suitable mathematical models (e.g. the Shallow Water Equations, SWE) and the quality level that can be obtained is potentially very good, the same is still not true for the computation of damage, a task for which there is not a single well-recognized methodology (Simonelli et al., 2022). The reasons are several: first, there is a different level of knowledge of the damage mechanisms leading to flood damage for the various elements at risk; this is reflected in an unbalanced availability of damage models for the various elements, with damage to residential buildings being the most investigated (Merz et al., 2010; Pregnolato et al., 2015; and Gerl et al., 2016). Second, damage mechanisms are strongly context-specific; this implies that models are hardly transferable in time and space (Molinari et al., 2020). Finally, the computation of damage requires the identification of items at stake and of their vulnerability: availability of data on these features may change from one context to another, further limiting models transferability and the range of models that can be adopted (Simonelli et al., 2022). In our opinion and experience, the marginal practical gain that could be obtained by improving the procedures for the computation of damage are larger than those that could be obtained by the improvement of current techniques for the solution of SWE. In this paper, based on the computed hazard, we present an instance of rigorous computation of the damage caused by the flood that followed the Gleno dam-break (December 1, 1923), considering the final, still undocumented part of the flood. The analysis of historical flooding events (e.g. Hesselink et al., 2003; Pilotti et al., 2011; Masoero et al., 2013; Petaccia and Natale, 2020; Aureli et al., 2021) has several reasons of interest. First, they are invaluable to make up our engineering experience of the consequences of an extreme event. Moreover, they provide unique real test cases to measure the predictive effectiveness and practical relevance of simplifying hypotheses in the mathematical and numerical foundation of adopted models. Finally, the match between observed and numerical results can be key to the acceptance of model results used for land planning and zonation by laypersons. The collapse of the Gleno dam caused havoc and a death toll of at least 350 lives along a 20 km long stretch of Valle di Scalve, a steep alpine valley, as far as the confluence with the large prealpine Valle Camonica. Whereas the propagation of the dam-break wave along the first 20 km stretch (Pilotti et al., 2011) was reproduced by using the first-order finite volume scheme proposed by Capart et al. (2003) that proved very effective for the narrow valley, we used HEC-RAS 2D to model the following bidimensional spreading of the wave on the alluvial fan (Milanesi and Pilotti, 2021) at the confluence with Valle Camonica. In that part of the simulation, we exploited a feature provided by HEC-RAS to model the sudden collapse of buildings and the dynamic modification of the computational domain. These two parts of the propagation were characterised by their impulsive nature. The following propagation along the 10 km long reach of Valle Camonica, where the flood wave moved as far as the entrance into deep Lake Iseo, causing extensive damages to levees, crops and isolated buildings, was more similar to a traditional flood and is documented for the first time in this paper. After reconstructing the original topography of the valley on the basis of a state-of-the-art algorithm (Van der Meulen et al., 2020) applied to a present-day LIDAR, complemented with original topographic maps and a rare aerial survey of the valley dating back to 1944, we study for the first time the effects of the propagation of the wave along Valle Camonica as far as the lake inlet. In this paper the hazard is computed by solving the 2D SWE on an unstructured grid with a proprietary WAF TVD finite volume solver never used in previous works. The implementation of a proprietary code gave the possibility to compute damage on the basis of the simultaneous values of water depth and velocity. Damage was assessed for human life and for 2 economic-related categories (agriculture and residential buildings) by implementing the MOVIDA (MOdello per la Valutazione Integrata del Danno Alluvionale) procedure (Ballio et al., 2022; Simonelli et al., 2022). The procedure was developed within a partnership of 8 Italian Universities, the National Research Council, and the Po River District Authority with the main objective of identifying the most appropriate exposure and flood damage models for all the assets listed in the EU "Floods" Directive, at the district level: population, infrastructures, economic assets (residential buildings, commercial and industrial activities, and agricultural activities), environmental and cultural heritage, and na-tech sites. The approach adopted in the procedure is based on the implementation of damage functions (Merz et al., 2010; Gerl et al., 2016) as the implementation of fragility functions (see e.g. Fuchs et al., 2019) is less appropriate considering the typology of analysed flood events (i.e. riverine flood) and the objective of the analysis (i.e. risk mitigation planning). The MOVIDA procedure has been used by the Po River District Authority to produce the damage maps at the basis of flood risk management in the district (see https://sites.google.com/view/movida-project for more information). By implementing state-of-the-art tools available in the literature, which are suitable for the Italian context, the procedure can be considered as the most advanced tool for the estimation of flood damage in the investigated context.

Considering that over the last 100 years Valle Camonica underwent a deep transformation from a purely agricultural area to one of the most deeply inhabited and industrialized valleys in the Italian pre-alpine area and considering that several large dams are still present in the surrounding mountains, we have eventually tested how the hazard and the damage would change if a similar flood wave occurred in the present situation. The analysis highlights the effects of the completed hydraulic works and of the changes in roughness over time along the river on the current distribution of hazard, showing that, as far as the expected damage is concerned, the decrease of hazard would be more than offset by the exponential increase of exposure in the floodplain surrounding the river.

2. The study case: the flooding of Valle Camonica by the Gleno Dam break

The Gleno dam (Valle di Scalve, Lombardy, north Italy, see Fig. 1) collapsed for structural deficiency 40 days after the first complete reservoir filling on December 1, 1923, releasing a volume of about 4.5 million m^3 of water. The flood wave took about 45 min to flush

the 20 km long stretch of steep and narrow valley between the dam and the village of Corna, located on the alluvial fan at the confluence with the larger and milder Valle Camonica, destroying everything along its way and causing a death toll of at least 350 people. Along this route, the peak discharge decreased by almost 90%, from about 21 000 m^3/s at the dam site to about 2700 m^3/s at the apex of the Corna alluvial fan. More details on this important test case and on its hydraulic modeling, accomplished by modifying the first-order finite volume numerical method proposed by Capart et al. (2003), are provided in Pilotti et al. (2011). The propagation on the Corna alluvial fan was then studied using HEC-RAS 2D, adapting the geometry of the computational domain to take into account the collapse of buildings during the simulation (Milanesi and Pilotti, 2021). At the confluence with the Oglio river, that drains Valle Camonica, the computed peak discharge decreased to about 2200 m^3/s due to the markedly bidimensional spread on the Corna alluvial fan. This value was still 1.6 times the T_{500} peak discharge at the same Oglio river station, as provided by official documents (AdbPo, 2016), although the reduced overall flood volume of about 4 million m^3 was only 10% of the expected T_{500} flood. Accordingly, an unusually steep and slim flood wave propagated for about 10 km along the wide and mild stretch of Valle Camonica, before entering the large (61 km^2) and deep (256 m) Lake Iseo (Pilotti et al., 2013). The wave caused a swift increase of the lake level that was measured at the lake outlet in Sarnico (see Fig. 1) along with the average outflowing discharge. Although in 1923 the event was widely

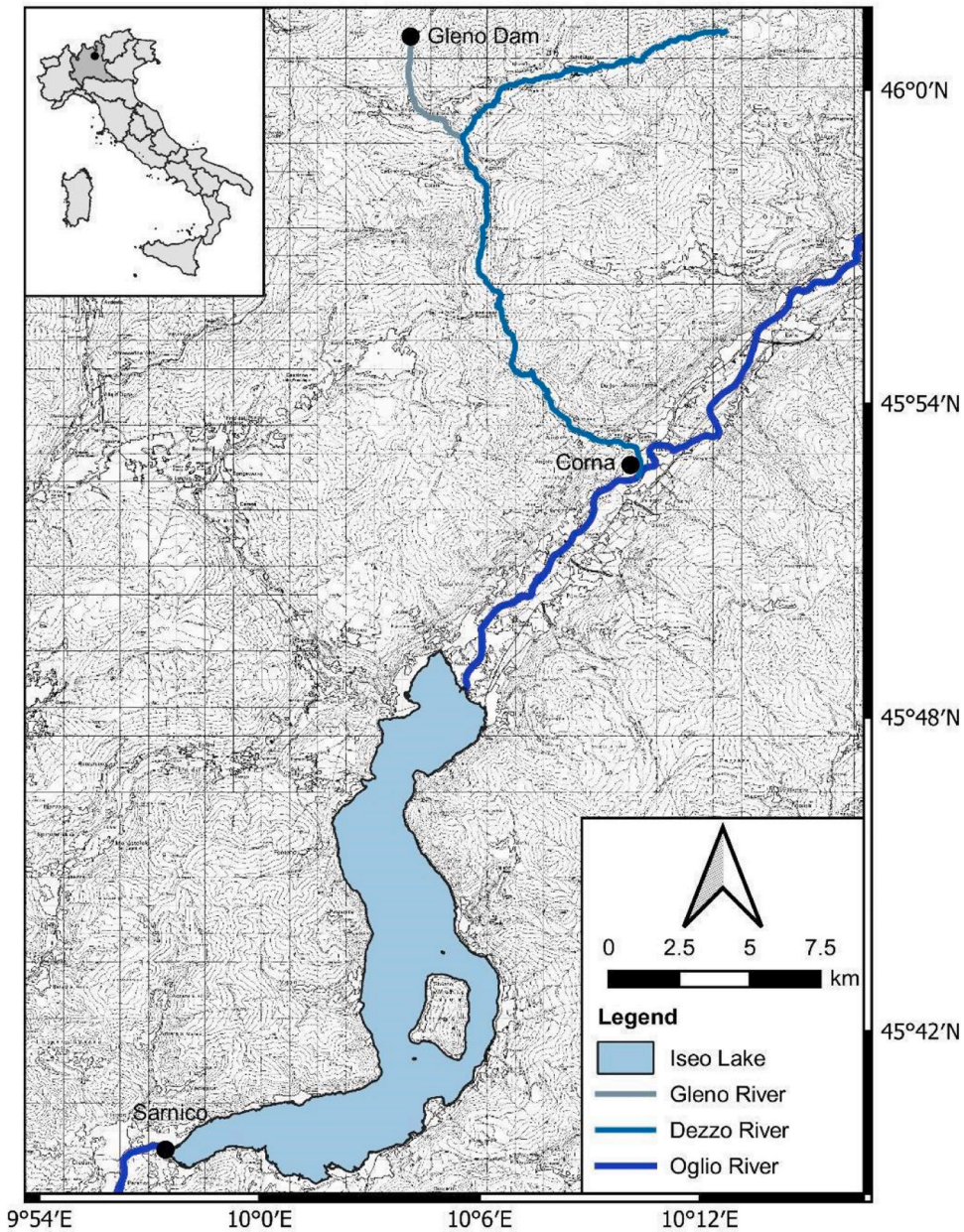

Fig. 1. The study area with the Oglio river and Iseo Lake. The black dots show the location of the Gleno dam and of the lake outlet at Sarnico.

covered by the Italian press, only a few documents have remained on the propagation along the downstream stretch of the Oglio river. In this area very few people died and only local information on the extent of the flooded area and a maximum measured water level in a flooded church are available. An extraordinary document, dating 1944 (see Fig. S2 of the supporting material), shows an aerial view of the whole Valle Camonica 21 years after the flood. This document provides the following important information for our study: 1) In 1944 (and, *a fortiori*, in 1923) Valle Camonica was still an agricultural area, with some farms located in the flooded area and crossed by a few roads and a railway. Historical documents show that the area was periodically affected by natural floods with significant impact on the local agricultural economy, characterized by the cultivation of corn, cereal crops, and orchards. 2) The planimetric layout of the Oglio river was very similar to the present one. 3) The riverbed was kept clean from trees and brushes. This could be expected because wood was traditionally the only material available for heating and cooking. The same situation is demonstrated by the pictures shown in Fig. S5 of the supplementary material that date back to the years around 1932. In its present situation (see Fig. S3 of the supplementary material) one can observe that over the last 100 years Valle Camonica has undergone a dramatic economic growth and that 1) Industrial activities have now a dominant role in the floodplain. 2) The riverbed is more distinctly separated from the surrounding floodplain. 3) Trees and bushes are systematically present along the river levees and even within the riverbed.

3. Methods

3.1. Finite volume discretization of 2D Shallow Water Equations

The system of 2D Shallow Water Equations (SWE) for mass and momentum balance can be written in conservative vectorial formulation as:

$$\mathbf{U}_t + \mathbf{F}(\mathbf{U})_x + \mathbf{G}(\mathbf{U})_y = \mathbf{S}(\mathbf{U})$$

$$\mathbf{U} = \begin{bmatrix} h \\ hu \\ hv \end{bmatrix},\ \mathbf{F}(\mathbf{U}) = \begin{bmatrix} hu \\ hu^2 + \frac{1}{2}gh^2 \\ huv \end{bmatrix},\ \mathbf{G}(\mathbf{U}) = \begin{bmatrix} hv \\ huv \\ hv^2 + \frac{1}{2}gh^2 \end{bmatrix},\ \mathbf{S}(\mathbf{U}) = \begin{bmatrix} 0 \\ -gh(S_{bx} + S_{fx}) \\ -gh(S_{by} + S_{fy}) \end{bmatrix} \tag{1}$$

where h [m] is the water depth, u and v [m/s] are the mean velocity components in x and y direction, g [m/s^2] is the acceleration of gravity, z_b[m] is the bed elevation, $S_{bx} = \partial z_b/\partial x$ and $S_{by} = \partial z_b/\partial y$ are the bed slope source terms S_{fx} and S_{fy} are the bed friction source terms, which can be written as a function of the Manning's coefficient. The following finite volume numerical scheme (e.g. Toro, 2001; Vázquez-Cendón, 2015) has been implemented to solve system (1). The entire computational domain Ω is divided into N triangular shaped control volumes K_i. The vector of conserved variables $\mathbf{U}$ is computed at the centre of gravity of each element, thus defining a cell-centred discretization. Following the approach defined in Ata et al. (2013), using an explicit Euler scheme and denoting the current time step as $t^n = n\Delta t$, system (1) can be approximated as:

$$\mathbf{U}_i^{n+1} = \mathbf{U}_i^n - \frac{\Delta t}{A_i}\sum_{j=1}^{m} \mathbf{H}(\mathbf{U}) \bullet \boldsymbol{n}_{ij} L_{ij} + \Delta t \mathbf{S}_i$$

$$\mathbf{U}_i = \frac{1}{A_i}\int_{K_i} \mathbf{U}(\boldsymbol{x}, t^n) d\boldsymbol{x},\ \mathbf{S}_i^n = \frac{1}{A_i \Delta t}\int_{t^n}^{t^n+\Delta t}\int_{K_i} \mathbf{S}(\mathbf{U}_i(\boldsymbol{x}, t)) d\boldsymbol{x} dt \tag{2}$$

where L_{ij} is the *j-th* side of the *i-th* cell, which is characterized by a normal vector $\boldsymbol{n}_{ij}$, while A_i is the area of the considered cell. Eq. (2) is obtained by the integration of Eq. (1) in the $(\boldsymbol{x} - t)$ space, i.e. $V = K_i \times [t^n, t^{n+1}]$. Furthermore $\mathbf{U}_i^n$ is the averaged spatial integral of the solution at time t^n and $\mathbf{S}_i$ is the volume integral average in V of the source term vector. To compute the intercell fluxes $\mathbf{H}(\mathbf{U}) = [\mathbf{F}(\mathbf{U})\ \mathbf{G}(\mathbf{U})]$ needed to update the conserved variables on the triangular grid, one can exploit the rotational invariance property of the system (Loukili and Soulaimani, 2007) between $\mathbf{F}$ and $\mathbf{G}$ over each side, which states:

$$\mathbf{H}(\mathbf{U}) \bullet \boldsymbol{n}_{ij} = \mathbf{T}_{n_{ij}}^{-1} \mathbf{F}\left(\mathbf{T}_{n_{ij}} \mathbf{U}\right),\ \mathbf{T}_{n_{ij}} = \begin{bmatrix} 1 & 0 & 0 \\ 0 & n_{ij,x} & n_{ij,y} \\ 0 & -n_{ij,y} & n_{ij,x} \end{bmatrix} \tag{3}$$

meaning that the computation of the fluxes reduces to a local 1D problem over each side:

$$\mathbf{U}_i^{n+1} = \mathbf{U}_i^n - \frac{\Delta t}{A_i}\sum_{j=1}^{m} \mathbf{T}_{n_{ij}}^{-1} \widetilde{\mathbf{F}}\left(\mathbf{T}_{n_{ij}} \mathbf{U}_i, \mathbf{T}_{n_{ij}} \mathbf{U}_j\right) L_{ij} + \Delta t \mathbf{S}_i \tag{4}$$

with $\widetilde{\mathbf{F}}\left(\mathbf{T}_{n_{ij}} \mathbf{U}_i, \mathbf{T}_{n_{ij}} \mathbf{U}_j\right) = \widetilde{\mathbf{F}}(\mathbf{U}_L, \mathbf{U}_R)$ being a discrete flux resolved using an exact or approximate solver of the Riemann problem having $\mathbf{U}_L$ and $\mathbf{U}_R$ as left and right initial states:

$$\begin{cases} \dfrac{\partial \mathbf{U}}{\partial t} + \dfrac{\partial \mathbf{F}(\mathbf{U})}{\partial x_n} = \mathbf{0} \\ \mathbf{U}(\boldsymbol{x}, 0) = \begin{cases} \mathbf{U}_L & x_n < 0 \\ \mathbf{U}_R & x_n > 0 \end{cases} \end{cases} \tag{5}$$

The application of the finite volume method requires a way to determine the numerical flux $\mathbf{F}(\mathbf{U})$ and the numerical source term $\mathbf{S}_i$. Here the numerical flux is computed using the Weighted Averaged Flux (WAF) approximation applied to a HLLC-type flux (Toro, 2001; Ata et al., 2013). The WAF scheme, being second-order accurate in space and time, produces spurious oscillations near steep gradients in the conserved variables (Loukili and Soulaimani, 2007). To suppress the unphysical oscillations while preserving the order of accuracy, a Total Variation Diminishing (TVD) nonlinear modification is enforced into the scheme (Toro, 2009). Enforcing this adaptation requires a wider spatial numerical stencil, i.e. the numerical flux now depends not only on the states present between the two considered cells ($\mathbf{U}_L$ and $\mathbf{U}_R$) but also on some upwinding cells necessary to suppress oscillations, which will be defined as $\mathbf{U}_{LL}$ and $\mathbf{U}_{RR}$. We have followed the approach described by Loukili and Soulaimani (2007) in which the upwind state variables are calculated using the neighbouring volumes. The discretization of the topography source term, i.e. S_{bx} and S_{by}, is key to ensure the quality of the results of the numerical scheme. Such discretization has to guarantee the well-balanceness property (the so-called *C-property*), meaning that non-trivial steady state solutions must be resolved correctly avoiding unphysical oscillations of the free surface (LeVeque, 1998). The procedure proposed by Audusse and Bristeau (2005) based on the hydrostatic reconstruction ensures both well-balanceness and positivity of the water depth and was selected to cope with the geometric source term given by the topography data. The same procedure was adopted also in Ata et al. (2013). Regarding the friction slope term, S_{fx} and S_{fy}, a semi implicit discretization scheme (Audusse and Bristeau, 2005; Ata et al., 2013) was implemented in order to handle instabilities caused by abrupt changes in water depth and velocity. Wet and dry fronts are handled by introducing a cutoff threshold of 10^{-5} m on the water depth to avoid unphysical velocities or instabilities. Boundary conditions are implemented by inserting *ad hoc* states corresponding to the type of boundary being modelled on the basis of the theory of characteristics (Hou et al., 2013; Yoon et al., 2004). The approach implemented in the current numerical scheme is the one followed by Hou et al. (2013) according to which solid wall or open boundary conditions can be imposed. The implemented code has been carefully validated with many analytical solutions and test cases that are available in the literature. In the supplementary materials (see Text S3), in order to show the shock-capturing capabilities of the proposed scheme, the performance of the code with the Ritter and the Stoker dam break problems is shown. Then the code is tested with the two-dimensional case of a radially symmetrical oscillating paraboloid (for which the analytical solution is available) testing the performance with moving wet/dry transitions. Finally, the performance of the code with a real test case is shown by reproducing the classic Malpasset dam break test case.

3.2. Reconstruction of the 1923 topography

The quality of the topographic description is a necessary prerequisite in the SWE solution process and in this case the reconstruction of the digital elevation model (DEM) representing the 1923 Valle Camonica topography is a crucial aspect in the test-case set-up. The comparison between historical maps and present satellite view shows that the planimetric path of the Oglio river is mostly unchanged, apart from a planimetric difference at the inlet of the lake that was introduced in the reconstruction of the 1923 topography. On the other hand, the floodplain surrounding the river was dramatically changed with the introduction of levees and roads on embankments that limit the expansion of a flood. Accordingly, we have removed the anthropic changes introduced over the last 100 years using the

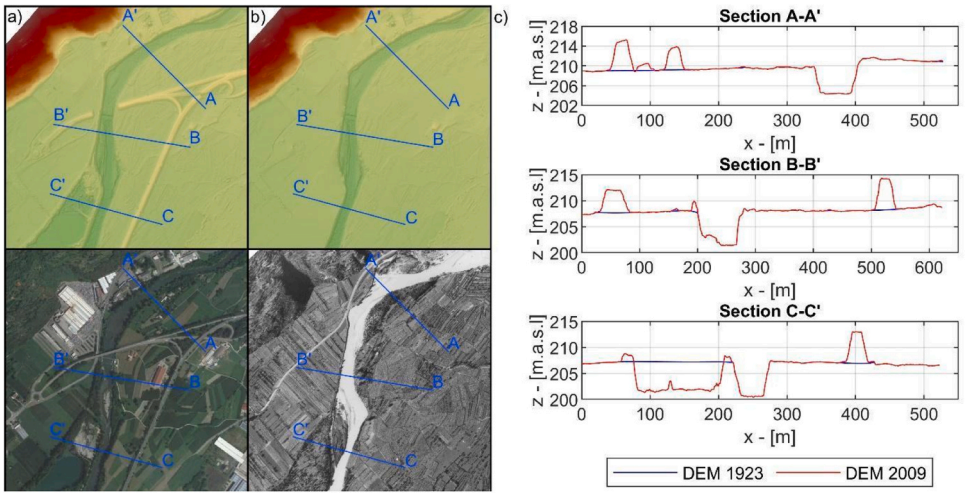

Fig. 2. a) DEM_2009 along with google satellite view; b) DEM_1923 along with a patch of the aerial photo of the valley taken in 1944 (© ICCD-Aerofototeca Nazionale, fondo RAF); c) comparison between DEM_2009 and DEM_1923 terrain profiles.

"top-down method" (Van der Meulen et al., 2020) which considers a high-resolution recent digital elevation model as a starting point from which each recently built element is removed one by one. Finally, the remaining void cells are interpolated using the surrounding elevations. The digital terrain model that was used for the present time simulations (DEM_2009 in the following) has a planimetric resolution of 0.8 m, was surveyed in 2008–2009 and has a planimetric and vertical accuracy of + /- 0.30 m and + /- 0.15 m respectively. The detailed steps followed to build the 1923 topography are provided in the supplementary material along with the details on the source and buffer width used in the removal process. An example of the results of the procedure is shown in Fig. 2 along with the corresponding patch of the 1944 aerial photo, the current topography, and a satellite view. The cross-sections extracted from the two different DEMs (DEM_2009 and DEM_1923) show an example of the profile of the terrain in correspondence of road embankments (section A-A′), of a levee (section B-B′) and of a recent quarry (section C-C′). Being limited downstream by a lake with small water level variations, the bed underwent no average aggradation or degradation. Accordingly, in the absence of old cross-section surveys, we did not modify the current riverbed.

3.3. Damage modelling

Due to their relevance in the test case, in this application, only three categories of the exposed elements were selected to produce a coherent comparison between the present and the 1923 scenario: population, residential building and agriculture. Damage estimation has been performed by means of the MOVIDA procedure (see introduction).

3.3.1. Population

According to 2007/60/EC the first indicator of the flood's adverse consequences must be related to the number of inhabitants affected by the flooding event. In this direction, the usual way to evaluate the damage to people is to compute the intersection between an exposure map (typically, the density of inhabitants) and the flooding extent. This is also done in the standard version of MOVIDA by combining hazard maps provided by hydraulic modelling with data coming from the Permanent Census of Population and Housing of the Italian National Institute of Statistics (ISTAT, 2011). However, it is important to underline that in this way the hazard is used only to limit the extent of the flooded area and not to pinpoint the real local vulnerability of human life. In other words, the highest damage level is provided by the maximum exposure, neglecting the effect of the actual local values of water depth and velocity on people safety. To overcome this limit, it can be assumed that a loss of stability of a person impacted, and potentially dragged away by the flow, can be used as a binary metric of human vulnerability (Pilotti et al., 2022). This can be done using the mechanical model proposed by Milanesi et al., (2015, 2016) who studied the stability of a person impacted frontally by a flow with velocity U and depth h through a physically based stability function that also considers the fluid density and the local ground slope. The human vulnerability is evaluated by the static stability, considering slipping and toppling modelled by the force equilibrium in the direction of the flow and by a moment equilibrium around the heel. Vulnerability to drowning is also considered, as a function of the maximum water depth. Finally, the three resulting stability thresholds can be combined together to find out the minimum admissible water depth for each given flow velocity. In this way, using literature parameters representing the physical features of children and of European adults, two vulnerability curves can be obtained: the upper one (conveniently approximated by Eq. 6) is valid for an adult and the lower one (approximated by Eq. 7) for a 7-year-old child:

$$h_{adults} = \min\left(1.4; \frac{2.809}{U + 1.102} - 0.416\right) \tag{6}$$

$$h_{children} = \min\left(1; \frac{1.565}{U + 0.884} - 0.275\right) \tag{7}$$

Moreover, considering that a large number of flood-related fatalities in urban areas are due to drowning of people in vehicles, the assessment of vehicles stability in a flood can be regarded as an additional criterion to assess people safety. To this end, Milanesi and Pilotti (2019) proposed a conceptual stability model for a stationary vehicle impacted by a flow explicitly accounting for the role of fluid density and of the sloping terrain. The model studied the equilibrium to slipping and was written in a dimensionless form in order to calibrate a set of lift and drag hydrodynamic coefficients representative not only of a single vehicle, as customary in most of the literature studies, but of a wide set of vehicles tested in laboratory conditions. Two easy to use approximate formulations of the stability limit as a function of the flow velocity U, depth h and of the local slope ϑ are given, for parallel and perpendicular relative orientation of the flow, as:

$$U \leq \left[\frac{(604 - 685\tan\vartheta - 1218h)\cos\vartheta}{38h + 1}\right]^{1/2} \tag{8}$$

$$U \leq \left[\frac{(390 - 443\tan\vartheta - 788h)\cos\vartheta}{68h - 1}\right]^{1/2} \tag{9}$$

Eq. (8) and Eq. (9) are defined for $0.158 < h < h_b$, where $h_b \approx 0.495$ m is the depth at which the vehicle starts floating in static water. Considering that the stability threshold for vehicles impacted by a flow in perpendicular orientation is more cautionary than the case of parallel direction, only Eq. (9) will be considered in the following analyses. The stability threshold for people and for vehicles provided by Eqs. (6), (7) and (9) can be easily combined to obtain conditions of growing vulnerability. For instance, in a five-level

grading in the (h, U) space (see Fig. 3a) they go from white (no vulnerability at all, point 0,0) to purple (maximum vulnerability) through yellow, orange and red. The V4 zone corresponds to areas where adult people life is challenged, V3 to areas where children life is challenged and V2 to areas where children are safe but not people in cars. Finally, the V1 zone corresponds to areas where also people in cars are safe.

The informative content of the graph shown in Fig. 3a can be used to compute the expected local physical damage to people by using the density of population as a metric of exposure. To this purpose the population density quartiles in the investigated areas can be computed and a colour grid that combines vulnerability with exposure can be built as shown in Fig. 3b. Here the roman numbers correspond to the population density quartiles. According to this classification, areas V4 where human life is at stake are ranked at the highest damage level (dark purple) independently from the population density. V1 areas have similar independence from population density and are ranked at the lowest damage level (dark yellow). Intermediate levels of vulnerability are affected by the population density. Note that for uniformity reasons we used Eq. (9) (i.e., the damage grading of Fig. 3b) also for the 1923 computations although its relevance was negligible at that time: this simplification implies that, for the 1923 case, the internal subdivision between V1 and V2 of the (h, U) field of stability for a child, has not the clear physical meaning that is retained for the 2022 map.

3.3.2. Residential Building

In the MOVIDA procedure the economic damage to residential buildings is computed as a function of the water depth, of the economic value of the buildings, and of some vulnerability parameters (see the supplementary material for details). In fact, the procedure neglects the destructive effect of the impulsive impact of a dam-break surge against a building (e.g., Milanesi et al., 2018). Whereas this effect was dominant on the alluvial fan of Corna (Milanesi and Pilotti, 2021), where the wave, channeled by the narrow gorge at the apex of the fan, hit buildings frontally, it soon became negligible during the propagation along Valle Camonica, where no building collapses were observed in the areas outside the river bed during the 1923 event. Accordingly, the MOVIDA procedure for residential buildings can be applied with confidence to the last part of the propagation of the Gleno dam break wave studied in this paper.

In MOVIDA, three different models are implemented: the Simple-INSYDE model (Galliani et al., 2020), the model proposed by Carisi et al. (2018) and the model proposed by Arrighi et al. (2018), all calibrated in the Italian context. The Simple-INSYDE model is a simplified version of the synthetic INSYDE model (IN-depth SYnthetic Model for Flood Damage Estimation, Dottori et al., 2016) that allows an easy implementation without significative loss of accuracy (Molinari et al., 2021). In this model the absolute economic damage to a single building is computed by the sum of the damage to the different harmed components of the building (i.e. storey, floor, basement, and boiler). Each component's damage is computed as a function of the relative damage, the footprint area of the building and the replacement value. The relative damage of the different building's components is evaluated by means of *ad-hoc* damage functions that depend on a set of vulnerability parameters (such as the level of maintenance, the finishing level, and the building structure), and two additional hazard parameters connected to the water depth, i,e, the duration of the flood and the presence of pollutants (for detail see Galliani et al., 2020). The second is a synthetic model proposed by Arrighi et al. (2018), where the relative damage to a building is computed with a piecewise linear function depending on the water depth only. The third is the empirical model proposed by Carisi et al. (Carisi et al., 2018; Amadio et al., 2019), in which the relative damage to a building is computed as a function of the maximum water depth (see the supplementary material for details). In the current scenario, data regarding the footprint area of

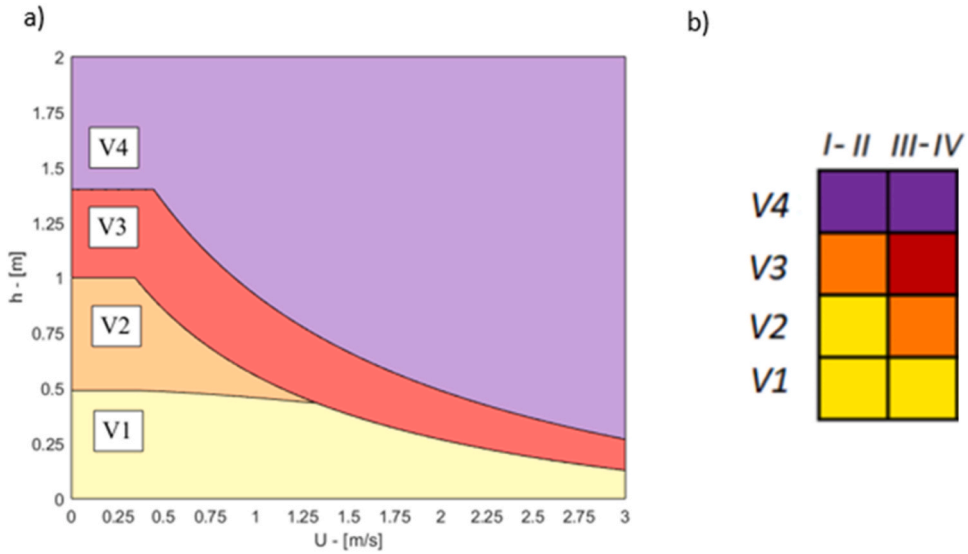

Fig. 3. a) Vulnerability space for people involved in floods, V4 zone: adult life in danger, V3 zone: child life in danger, V2 safe for a child life but not for people in cars and V1 zone: people in cars are safe. b) final damage grading obtained by combining the classes of growing vulnerability of 3a) with the population density quartiles.

the buildings, the number of floors, and the building use were extracted from the topographic database of the Lombardy Region. Information on the building structure and the level of maintenance was retrieved from ISTAT, aggregated at the census block scale. Then, the most frequent values of building structure and level of maintenance were assigned at each building which fell inside the considered census block. The replacement value was provided by Centro Ricerche Economiche Sociologiche e di Mercato nell'Edilizia (CRESME), actualized at the present time (AdBPo, 2021). In the 1923 scenario, the footprint area of the few existing buildings in the flooded area was extracted from the same regional topographic database. The number of floors and the building use was assumed to be unchanged between the two scenarios. We assumed that all the buildings inside the domain were characterized by the masonry structure that is typical of the alpine mountain area and by a low level of maintenance, in accordance with the relatively poor agricultural economy in the valley. To compare the economic damage, we used in both the scenarios the same replacement value provided by CRESME. All the vulnerability parameters used for the computation of the damage and the sources are summarized in the supplementary material.

3.3.3. *Agriculture*

In the MOVIDA procedure, damage to the agricultural sector is evaluated by the AGRIDE-c model (Molinari et al., 2019). The model estimates the damage to the main crops in northern Italy (maize, wheat, barley, grassland, and rice) in terms of reduction of the income of the farmers because of a flooding event. This means that damage to other agricultural components like equipment and livestock are neglected. With respect to the former, this choice is linked to the evidence that, to our knowledge, there is no available data to evaluate their spatial distribution and their exposed value in a homogeneous and reliable way, nor models to estimate the expected flood damage (at least, for the Italian context). Regarding livestock, their presence in the investigated area is negligible. Still, we found no sources to evaluate their exposure in the historical scenario. Consequently, expected damage to the agricultural sector could be underestimated.

A regionalized version of the original model was developed in MOVIDA, considering the averaging yields, prices, and production costs in the Po River District (AdBpo, 2021). The input variables required by AGRIDE-c include: the water depth (provided by the hazard maps), the duration of the flood, the area occupied by the crops, the type of crops cultivated in each area, the time of the flood during the year and the alleviation strategy adopted by farmers. In the current scenario, the cultivated area was derived by coupling the cadastral maps and the type of the crops obtained from farmers' declarations. It is difficult to have the same detailed data for the

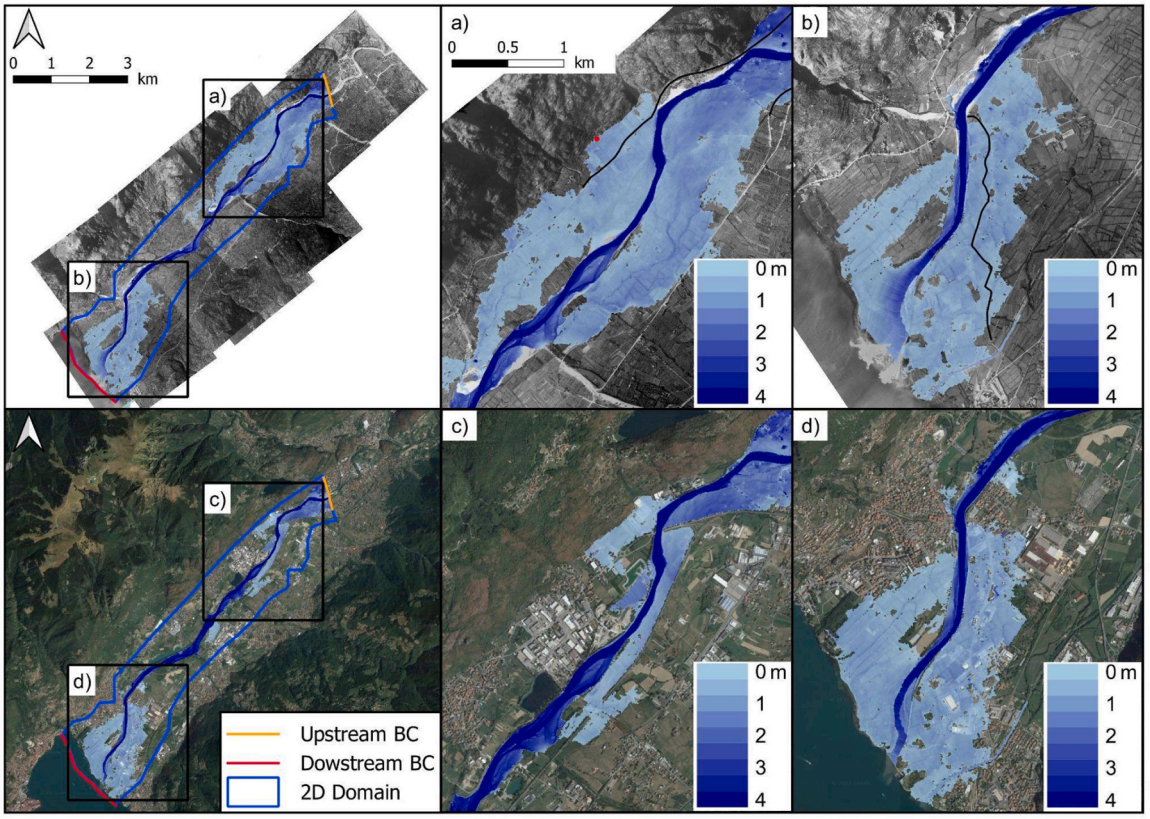

Fig. 4. Envelope of the maximum non-simultaneous water depths computed using DEM_1923 (upper row) and DEM_2009 (lower row). Figures a, c and b, d show an enlarged view of the area downstream of Corna and upstream of Lake Iseo. The solid black lines reported on a) and b) show two locations where the presence of the water is historically documented and the red dot is the location of the flooded church.

1923 scenario, so some kinds of simplifications were unavoidable. The area occupied by the crops was defined using the Land Cover shapefile derived from the aerial survey carried out in 1954. In this map, the land cover is classified with the classes of the CORINE land cover project and according to this classification, the arable land and pastures were considered as agricultural areas covered by crops of wheat, corn and grassland. As will be shown in the following, the duration of the flood in the river was limited to a few hours and, according to the historical documents, the surrounding floodplain was flooded for a few days. On the other hand, according to the table of AdBpo (2021), in winter the damage per unit area of each crop type remains constant for flood duration shorter than five days. Accordingly, we assumed in both scenarios that the flood occurred in December with an overall duration of 2 days.

4. Results

4.1. Wave propagation along the floodplain as far as the lake inlet

The upstream boundary condition for the 2D SWE solver is provided by the flood hydrograph at the foothill of Corna computed by Milanesi and Pilotti (2021), that was superimposed to the Oglio base flow of 180 m^3/s, documented at Sarnico (the lake outlet) the day before the event. The downstream boundary condition was provided by the average level of the lake during the month of December, set to 185.75 m a.s.l. The aerial survey (see Fig. S2 in supplementary material) suggests a riverbed clear of bushes and trees for the 1923 scenario. Although Fig. S2 shows the condition of the river in 1944, one can expect that it did not significantly differ from the situation of 1923 (see also Figs. S5 and S6 which dates back to 1932 and 1940), as a consequence of the local extensive use of wood for heating and cooking that characterized the first half of the 20th century. Accordingly, a lumped Manning coefficient of 0.05 $s/m^{1/3}$ was assumed, while in the floodplain 0.067 $s/m^{1/3}$ was adopted considering the presence of short vegetation in the fields. In the present scenario, a more in-depth characterization of the land use was available (see Fig. S4) which guided the zonation of the friction coefficient across the domain, also using the information provided by some satellite images. Friction coefficient for the riverbed ranged between 0.033 $s/m^{1/3}$ and 0.1 $s/m^{1/3}$. One of the advantages of the unstructured mesh used in the implemented solver is the ability to adjust the grid size to the geometry of the domain. In this application, the centres of the computational cells that are inside the riverbed have an average distance of 1.5 m which becomes 3 m in external areas for a total of 236 327 cells covering an area of around 16 km^2 (see also Fig. S9 in the supplementary material). The mesh in the areas inside the riverbed and in the inundated areas has been refined up to the point of obtaining a substantial independence of the results with respect to further refinements.

Fig. 4 shows the maximum extent of the flooding using the topography provided by DEM_1923 (upper row) and DEM_2009 (lower row). The extension of the flooded area in the 1923 scenario is 7.09 km^2 and 4.82 km^2 in the 2022 scenario. The computed h map for the 1923 event is in agreement with the only documented water mark in the flooded area (computed average water level 1.00 m,to be compared with the recorded level in the church 1.2–1.5 m) and with the documented extensive flooding of the two main roads, shown as solid black lines in Fig. 4a and b. Everywhere in the domain the present flood extent is smaller than the 1923 one. The comparison of the two maps shows that after 100 years, the river training works (first of all an important levee built on the first river bend on the right riverbank) and the construction of the highway levee on the hydrographic left side have strongly reduced the extent of the flooding in the upper part of the domain. In the lower portion of the domain the reduction of the hazard is smaller. On the other hand, the exposure in the flooded areas (see Fig. 4c and d) shows a dramatic increase.

Fig. 5 shows the hydrograph at the upstream end of the domain along with the computed hydrographs at the entrance to Lake Iseo. It is interesting to observe the strong peak reduction that is caused by lateral flooding, reinforced by the river geometry and roughness, during the propagation of the small volume of the short flood wave. Whereas the initial peak discharge at Darfo was 1.6 times the

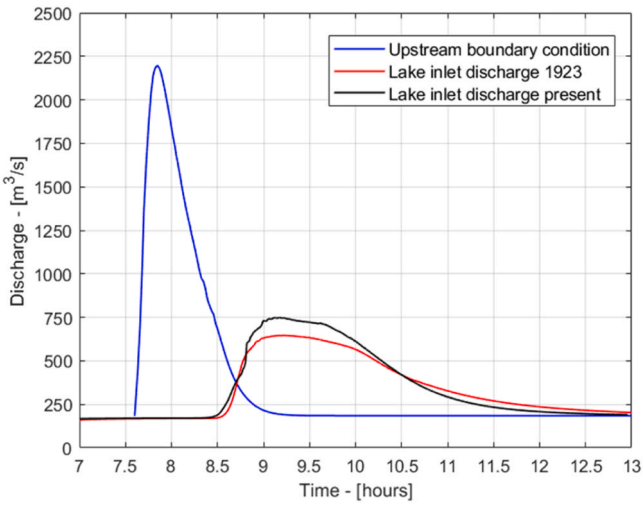

Fig. 5. Hydrographs comparison. The blue solid line is the upstream boundary condition. The red and black solid lines represent the computed discharge hydrographs entering the lake in the 1923 and present-day scenario.

corresponding T_{500} peak discharge, upstream of frame b) and d) in Fig. 4 the computed peak discharge (996 m^3/s and 1240 m^3/s for the 1923 and 2022 event, respectively) was already within the bounds of a T_{200} peak discharge (1160 m^3/s in Darfo, AdbPo, 2016). Eventually, at the lake inlet the peak discharge was comparable to a T_{20} peak discharge (710 m^3/s, AdbPo, 2016). Accordingly, moving from Darfo to the lake inlet, the wave progressively transformed into an ordinary hydrological flood. Moreover, as one could expect, the peak reduction is stronger in the 1923 setting, showing the dominance of lateral flooding with the 1923 topography, with respect to the increase of the river bank roughness that characterizes the 2009 scenario.

4.2. Computation of damage

4.2.1. Population

In the flooded area the density of inhabitants within elementary units called census blocks was chosen as a proxy of the population exposure (E). In the studied zone the average area of these units is 0.33 km^2 ranging between 775 m^2 and 2.50 km^2. Accordingly, the exposure is provided by the uniform density of population within each unit. On the other hand, the population census of 1921 counted the inhabitants at the municipal scale, which could lead to the assumption of uniform density of inhabitants within each municipality. However, in the considered mountain area most of municipality surface is unpopulated and a better distribution of the population at the census unit scale can be obtained by distributing the population according to the Land Cover shapefile derived from an aerial survey carried out in 1954. As observed above, when the population density is known, the damage can be computed either on the basis of the flooded extent only or after using Eqs. (6), (7) and (9) to compute the local vulnerability. Whenever a local vulnerability function of water depth and velocity is introduced as a dynamic indicator, its maximum value must be computed along the simulation using synchronous local values of velocity U and depth h. However, most SWE commercial solvers only provide the envelope maps of maximum water depth and velocity, whose use leads to an overestimation of vulnerability because h and U maxima do not necessarily occur simultaneously during the flood. For instance, if one considers the filling of a depression, maximum velocity might occur at the beginning, when the depth is small, and the maximum depth at the end, when the velocity tends to zero. However, it is difficult to evaluate a priori the extent and the practical relevance of this overestimation. In order to provide a quantitative insight on this issue, our SWE solver computed the vulnerability at each time step of the simulation, keeping track of its maximum value. Finally, the vulnerability was also computed with the envelope maps of (h, U) maxima, providing a quantification of the error. The results are shown in Fig. 6. As one can observe local overestimations (up to 3 classes) can be reached, although limited to a small fraction of the involved area.

Accordingly, the results show that the actual relevance of this error depends on the scale of representation of the damage. When a catchment scale is used, the local scale is typically too fine and, for practical reasons, the vulnerability results are averaged at the scale dictated by the resolution of the population density. In such a case, the error would become irrelevant. On the other hand, if local information is required (e.g. at the municipal level for local planning or for civil protection measures) we believe that this error must be considered. Obviously, the error depends on the specific case and on the choice of the vulnerability thresholds. However, considering that the selected thresholds are physically based and that the flood is an extreme one, we believe that the obtained results provide informative indications also for other practical cases. The damage maps for 1923 and for present day, obtained by averaging the vulnerability at the population density scale, are shown in Fig. 7.

Fig. 7a and c show the "business as usual" approach, i.e. are obtained considering the flooded areas as a metric of hazard and the density of population as a metric of exposure. The damage for people is graded using the population density in flooded areas: white (unpopulated zones), yellow (I quartile), orange (II quartile), red (III quartile), and dark purple (IV quartile). On the other hand, in Fig. 7b and d the damage is graded considering the actual physical vulnerability of people and the population density quartiles shown

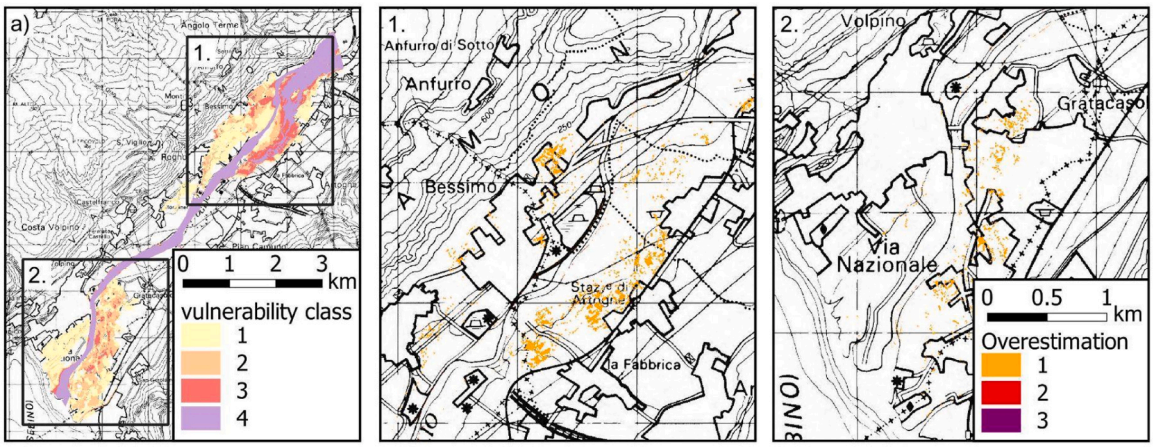

Fig. 6. 1923 Scenario a) Maximum vulnerability computed at each time step as a function of synchronous water depth and velocity. On the right, 1. and 2. show, for the two rectangular patches, the difference between maximum vulnerability computed as a function of the envelope of maximum water depth and velocity and maximum vulnerability correctly computed at each time step as a function of synchronous water depth and velocity.

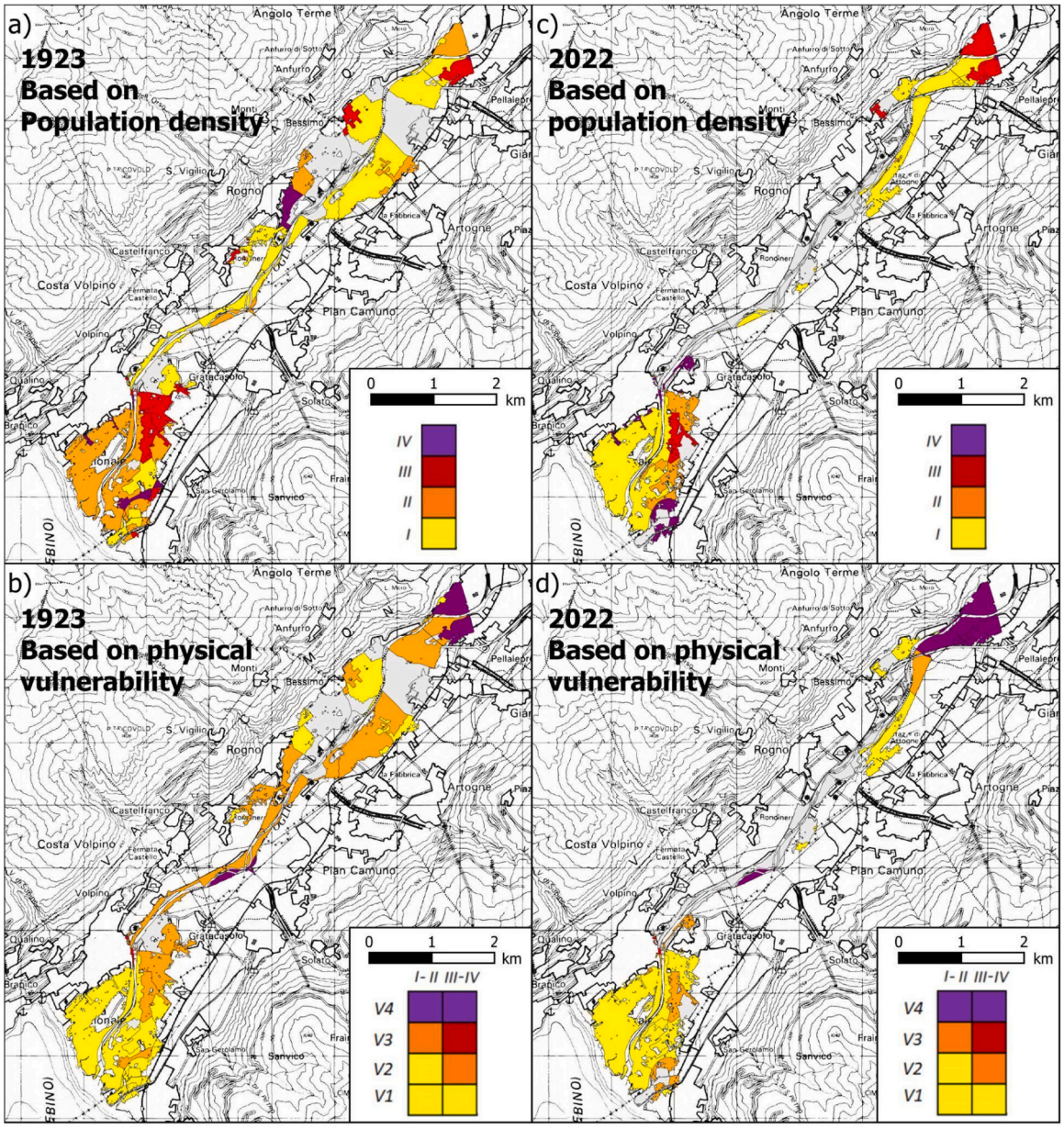

Fig. 7. 1923 and 2022 damage maps for population computed using the extent of flooding only (a, c) and taking into account the actual hazard within the vulnerability functions (6), (7) and (9) (b, d).

in Fig. 3b.

It is important to observe that, using the density of the population as a single metric, the zone with maximum damage is where the population density is highest, independently from the actual hazard intensity. For instance, in the 1923 scenario, the damage would be highest where the real vulnerability is lowest. On the contrary, the zone at maximum damage in the 1923 and 2022 map produced with the proposed approach is in the upper part of the domain where the actual vulnerability is highest, as shown in Fig. 6.

4.2.2. Residential buildings

According to the MOVIDA procedure, the damage was computed for each flooded building with the three proposed models. The selected damage index is the monetary damage density, computed as the ratio between the mean value of the monetary damage provided by the three different models aggregated at the census block scale and the area of the census block (Fig. 8), where shadings show the expected damage density within each census block.

As one could expect, the damage in the present scenario is much larger due to the increase of exposure. The exposed buildings in the 1923 (2022) scenario were 80 (562) and the economic exposure computed was 24.92 M€ (175.26 M€).

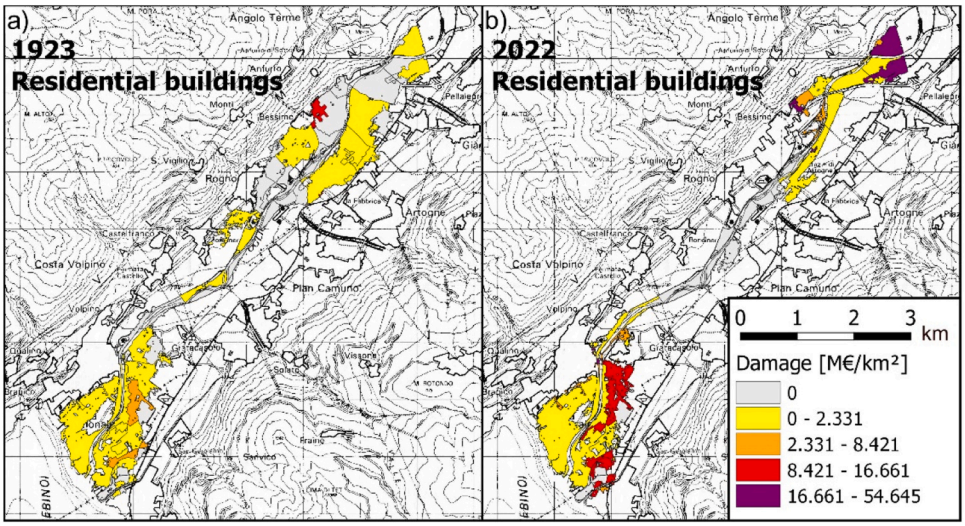

Fig. 8. Monetary damage density for the residential buildings: a) 1923 scenario, b) 2022 scenario.

4.2.3. Agriculture

The damage to the agricultural sector was computed using the hazard provided by the computed water depth only. The damage index produced by the MOVIDA procedure (Fig. 9) is the monetary damage density computed for each census block.

The total damage computed by the procedure for the 1923 (2022) scenario was 253 923 € (55 091 €), in accordance with a reduction of agricultural land occurred from 1923 to the present day. It is important to notice that the time when the flood occurs strongly affects the results in accordance with the vegetative stage of the affected crops. The Gleno accident occurred in winter when most of the crops are at rest; would the event occurred in another season, damage to agriculture could be significantly higher.

4.2.4. Overall expected economic damage

The maps shown in Fig. 8 and Fig. 9 are dimensionally coherent and can be summed to produce the overall economic damage map for each scenario shown in Fig. 10.

Incidentally, in the considered case the monetary damage for the agricultural sector is negligeable with respect to the residential damage.

5. Final discussion

In this paper we present a comprehensive quantitative evaluation of flood damage with reference to a real historical case,

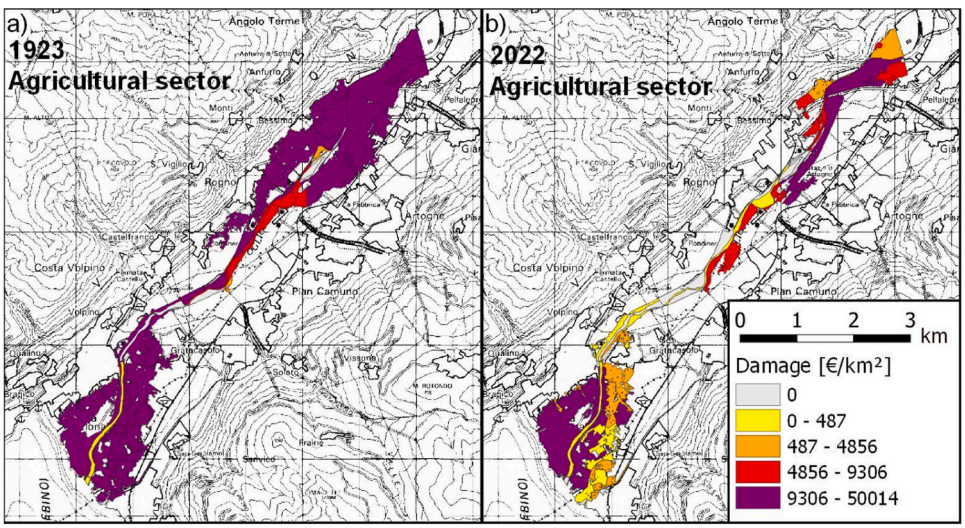

Fig. 9. Monetary damage density for the agricultural sector: a) 1923 scenario, b) 2022 scenario.

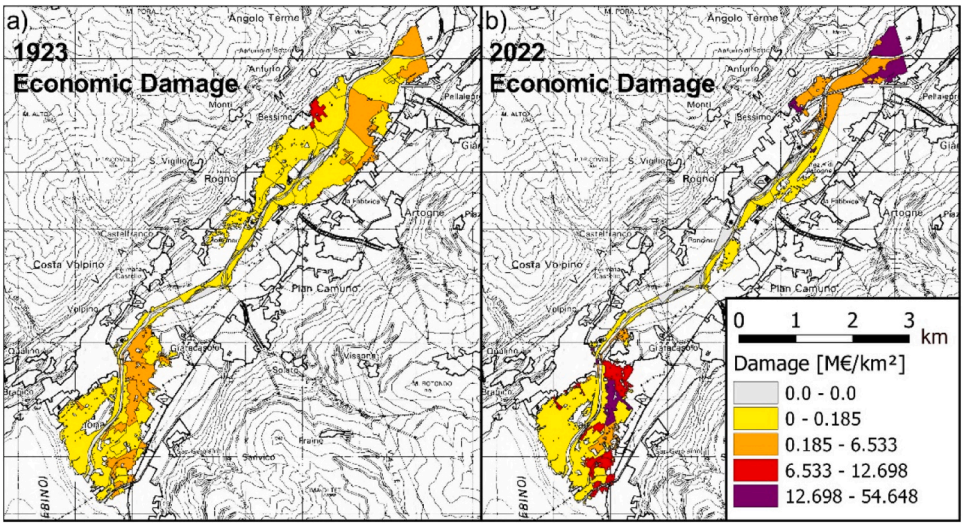

Fig. 10. Total monetary damage density for the agricultural and residential sector a) 1923 scenario, b) 2022 scenario.

considering the final part of the propagation of the dam-break wave caused by the collapse of the Gleno dam in 1923. Accordingly, we use quantitative methodologies for the numerical solution of the flow field and for the evaluation of damage.

The paper focused on the expected impact on population, agriculture and buildings. Although these were the most relevant elements at the time of the event and in the present scenario, the approach that we adopted for their estimation has some limitations. For instance, regarding damage to people, we neglected the influence of refuge behaviour of the population on the potential life loss (e.g. Wei et al., 2021, 2022): however, such information is essential only in the contingency planning phase and requires data at the microscale level (e.g. on alert times, on the social and physical vulnerability of individuals, on evacuation plans, etc.) which are difficult to recover, especially for the historical scenario. Moreover, the computation of damage to buildings is based on the MOVIDA procedure, which neglects the role of flow velocity on buildings. Accordingly, this procedure would be unsuitable in presence of strongly impulsive events, like the one that characterised the propagation of the wave upstream of its confluence in the Oglio River. Actually, the strong peak attenuation undergone by the Gleno dam-break wave after its confluence in Valle Camonica soon transformed this peaked and short flood wave into a flood comparable to a hydrological one.

Other limitations of the work are linked to neglected elements, such as infrastructures and economic activities (including stocks). Their exposure in the present scenario is limited while they were, in fact, absent in the historical one. This is the main reason that led us to exclude them from the assessment, along with the limited reliability of available damage models for these elements in comparison to those included in the analysis (see also https://sites.google.com/view/movida-project). Accordingly, the results of the hazard and damage mapping performed in this study can be used to appreciate the effect of the hydraulic works accomplished along the river after the Gleno accident for the control of hydrologic floods, highlighting that the designed reduction of flood hazard has been more than offset by the increase of exposure in the floodplain surrounding the river, leading to a present situation of higher risk than in the past. It is worth noting that the consideration of exposed infrastructure and economic activities in the damage assessment would have strengthened this result.

On the other hand, depicting the present risk situation, they can be used as the informative base for prevention and preparedness activities required by flood risk management. In this perspective, obtained results assume a different significance (Molinari et al., 2014) according to the objective of the analysis. Also with respect to preparedness, the vulnerability of people, computed using physically based methods, should be considered as the dominant criterion when the flood warning time is short with respect to the time of implementation of civil protection measures. This situation is typical of mountain areas, which are characterized by impulsive events, such as flash floods or debris flows, with potentially catastrophic consequences on the downstream areas. In the planning of long-term mitigation actions, guaranteeing the safety of people still assumes high significance (as indicated by the same Floods Directive); still, the benefit of alternatives of intervention should also consider the potential reduction of economic damage (focusing on potentially high damaged areas), in a multi-criteria approach. The implications of flood risk mapping are therefore huge both from the social and economic point of view. Accordingly, every effort directed to the improvement of the criteria used in this task is widely justified. Our experience shows that these criteria must exploit all the available information on hazard, exposure and vulnerability and be based on rational models, which are the only ones that can be justified in the inevitable confrontation with stakeholders. As obvious as it may seem, this prerequisite is not common in the current fragmented flood-risk calculation framework. The approach adopted in this work could then be considered as a best practice to be replicated in similar flood risk assessment problems.

6. Conclusions

This paper presents a detailed example of computation of flood damage, cast within the reconstruction of the final part of the

historical Gleno dam-break event (occurred in the Italian alps in 1923), characterised by the propagation through a large alpine valley. A new 2D SWE solver was implemented to numerically reconstruct the flood. The solver was also used to test the relevance of the practice of using the envelope of maximum velocity and depth in the computation of vulnerability functions and to compare the original hazard scenario with the situation that would result should the same event occur nowadays.

A detailed and comprehensive procedure was implemented to compare the damage in the two considered scenarios. The use of physically based vulnerability functions for people provides damage maps that are significantly different from the ones that would be obtained considering only the flood extent and the population density, as customary in many implementations worldwide. This result emphasizes the importance of including all the information available on the physics of the process.

The application of the SWE solver using the topography of the current floodplain and the one reconstructed for the 1923 setting, shows the reduction of the hazard following the hydraulic works built along the river. However this effect has been more than offset by the increase of exposure in the surrounding floodplain, leading to a present situation of higher risk than in the past. Obtained results are significant both from a social and economic point of view. On one hand, they highlight the limitations of the policies adopted in the past for the reduction of the flood risk in the analyzed area, that mostly relied on structural interventions without addressing the issue of reducing built-up spaces in floodplain areas, a difficult task under the pressure of the strong economic development occurred in the last century in Italy. On the other hand, they show that the consequence of a similar dam-break event that would occur nowadays could be huge, both from the point of view of people affected and of economic damage. In this respect, obtained risk maps can support the development of preparedness and prevention activities in the area. Despite some limitations in the evaluation of flood damage, mainly linked to a partial availability of damage models and required data, the approach followed in the paper proved to be highly informative for risk management decision problems and should be replicated in contexts similar to the one here investigated.

CRediT authorship contribution statement

Riccardo Bonomelli: Conceptualization, Methodology, Software. **Gabriele Farina:** Methodology, Software. **Marco Pilotti:** Conceptualization, Supervision, Methodology. **Daniela Molinari:** Methodology. **Francesco Ballio:** Methodology, All: Writing - Original draft preparation; Writing - Review & Editing.

Data Availability

Data will be made available on request apart from material belonging to third parties that we have no permission to share.

Acknowledgements

The permission to use the following pieces of information is kindly acknowledged: Aerial picture of Figs. 2, 4 and S2, provided by ICCD-Aerofototeca Nazionale, fondo RAF, volo 1944, authorized by Istituto Centrale per il Catalogo e la Documentazione –MiC. DEM_2009, provided by the Italian Ministry for the Environment, Land and Sea. We thank the Reviewers for their valuable suggestions and thoughtful comments that contributed to the improvement of the paper.

This work is part of the research activities of the MOVIDA group and was made possible by the 2 following projects: 1) Assessment of Cascading Events triggered by the Interaction of Natural Hazards and Technological Scenarios involving the release of Hazardous Substances (Grant No. 2017CEYPS8) funded by the Italian Ministry of Education, Universities and Research. 2) RETURN Extended Partnership, funded by the European Union Next-GenerationEU (National Recovery and Resilience Plan – NRRP, Mission 4, Component 2, Investment 1.3 – D.D. 1243 2/8/2022, PE0000005).

Appendix A. Supporting information

Supplementary data associated with this article can be found in the online version at doi:10.1016/j.ejrh.2023.101467.

References

AdbPo, 2016. Piano per la valutazione e la gestione del rischio di alluvioni: Profili di piena dei corsi d′acqua del reticolo principale, Marzo 2016.

AdBpo, 2021. Relazione metodologica: MOdello per la Valutazione Integrata del Danno Alluvionale (MOVIDA) Distretto del fiume Po dicembre 2021 (⟨www.pianoalluvioni.adbpo.it⟩).

Amadio, M., Scorzini, A.R., Carisi, F., Essenfelder, A.H., Domeneghetti, A., Mysiak, J., Castellarin, A., 2019. Testing empirical and synthetic flood damage models: the case of Italy. Hazards Earth Syst. Sci. 19, 661–678. https://doi.org/10.5194/nhess-19-661-2019.

Arrighi, C., Rossi, L., Trasforini, E., Rudari, R., Ferraris, L., Brugioni, M., Franceschini, S., Castelli, F., 2018. Quantification of flood risk mitigation benefits: a building-scale damage assessment through the RASOR platform. J. Environ. Manag. 207, 92–104. https://doi.org/10.1016/j.jenvman.2017.11.017.

Ata, V., Pavan, S., Khelladi, S., Toro, E.F., 2013. A Weighted Average Flux (WAF) scheme applied to shallow water equations for real-life applications. Adv. Water Resour. 62, 155–172. https://doi.org/10.1016/j.advwatres.2013.09.019.

Audusse, E., Bristeau, M.O., 2005. A well balanced positivity preserving second order scheme for shallow water flows on unstructured meshes. J. Comput. Phys. 206, 311–333. https://doi.org/10.1016/j.jcp.2004.12.016.

Aureli, F., Maranzoni, A., Petaccia, G., 2021. Review of historical dam-break events and laboratory tests on real topography for the validation of numerical models. WATER 13 (14). https://doi.org/10.3390/w13141968.

Ballio. F. Armaroli. C. Arosio. M. Arrighi. C. Borgogno-Mondino. E. Carisi.F. et al. The MOVIDA Project to Support the Update of Flood Risk Maps in the Po River District: methodology for flood damage assessment 2022.https://doi:10.3850/IAHR-39WC2521711920221136.

Capart, H., Eldho, T.I., Huang, S.Y., Young, D.L., Zech, Y., 2003. Treatment of natural geometry in finite volume river flow computations. J. Hydraul. Eng. 129 (5), 385–393.

Carisi, F., Schröter, K., Domeneghetti, A., Kreibich, H., Castellarin, A., 2018. Development and assessment of uni- and multivariable flood loss models for Emilia-Romagna (Italy). Nat. Hazards Earth Syst. Sci. 18, 2057–2079. https://doi.org/10.5194/nhess-18-2057-2018.

Dottori, F., Figueiredo, R., Martina, M.L.V., Molinari, D., Scorzini, A.R., 2016. INSYDE: a synthetic, probabilistic flood damage model based on explicit cost analysis, 2577–259 Nat. Hazards Earth Syst. Sci. 16. https://doi.org/10.5194/nhess-16-2577-2016.

Fuchs, S., Keiler, M., Ortlepp, R., Schinke, R., Papathoma-Köhle, M., 2019. Recent advances in vulnerability assessment for the built environment exposed to torrential hazards: Challenges and the way forward. ISSN 0022-1694 J. Hydrol. Volume 575, 587–595. https://doi.org/10.1016/j.jhydrol.2019.05.067.

Galliani, M., Molinari, D., Ballio, F., 2020. Brief communication: simple-INSYDE, development of a new tool for flood damage evaluation from an existing synthetic model. Nat. Hazards Earth Syst. Sci. 20, 2937–2941. https://doi.org/10.5194/nhess-20-2937-2020.

Ge, Wei, Jiao, Yutie, Wu, Meimei, Li, Zongkun, Wang, Te, Li, Wei, Zhang, Yadong, Gao, Weixing, Gelder, Pieter van, 2022. Estimating loss of life caused by dam breaches based on the simulation of floods routing and evacuation potential of population at risk. J. Hydrol. Volume 612 (Part A, 2022), 128059 https://doi.org/10.1016/j.jhydrol.2022.128059.

Gerl, T., Kreibich, H., Franco, G., Marechal, D., Schröter, K., 2016. A review of flood loss models as basis for harmonization and benchmarking. PLoS ONE 11, e0159791. https://doi.org/10.1371/journal.pone.0159791.

Hesselink, A.W., Stelling, G.S., Kwadijk, J.C.J., Middelkoop, H., 2003. Inundation of a Dutch river polder, sensitivity analysis of a physically based inundation model using historic data. Water Resour. Res. 39 (9), 1234. https://doi.org/10.1029/2002WR001334.

Hou, J., Simons, F., Mahgoub, M., Hinkelmann, R., 2013. A robust well-balanced model on unstructured grids for shallow water flows with wetting and drying over complex topography. Comput. Methods Appl. Mech. Eng. 257, 126–149. https://doi.org/10.1016/j.cma.2013.01.015.

ISTAT - Istituto Nazionale di Statistica (2011). Censimento della popolazione e delle abitazioni. Available at: ⟨https://www.istat.it/it/censimenti-permanenti/censimenti-precedenti/popolazione-e-abitazioni/popolazione-2011⟩.

LeVeque, R.J., 1998. Balancing source terms and flux gradients in high-resolution Godunov methods: the quasi-steady wave-propagation algorithm. J. Comput. Phys. 146, 346–365. https://doi.org/10.1006/jcph.1998.6058.

Loukili, Y., Soulaimani, A., 2007. Numerical tracking of shallow water waves by the unstructured finite volume WAF approximation. Int. J. Comput. Methods Eng. Sci. Mech. 8, 1–14. https://doi.org/10.1080/15502280601149577.

Masoero, A., Claps, P., Asselman, N.E., Mosselman, E., DiBaldassarre, G., 2013. Reconstruction and analysis of the Po River inundation of 1951. Hydrol. Process. 27, 1341–1348. https://doi.org/10.1002/hyp.9558.

Merz, B., Kreibich, H., Schwarze, R., Thieken, A., 2010. Review article "Assessment of economic flood damage". Nat. Hazards Earth Syst. Sci. 10, 1697–1724. https://doi.org/10.5194/nhess-10-1697-2010.

Milanesi, L., Pilotti, M., 2019. A conceptual model of vehicles stability in flood flows. *J. Hydraul. Res.*, *IAHR* 58 (4). https://doi.org/10.1080/00221686.2019.1647887.

Milanesi, L., Pilotti, M., 2021. Coupling flood propagation modeling and building collapse in flash flood studies. J. Hydraul. Eng., ASCE. https://doi.org/10.1061/(ASCE)HY.1943-7900.0001941.

Milanesi, L., Pilotti, M., Ranzi, R., 2015. A conceptual model of people's vulnerability to flood. Water Resour. Res. 51, 182–197. https://doi.org/10.1002/2014WR016172.

Milanesi, L., Pilotti, M., Bacchi, B., 2016. Using web-based observations to identify thresholds of a person's stability in a flow. Water Resour. Res. 52 https://doi.org/10.1002/2016WR019182.

Milanesi, L., Pilotti, M., Belleri, A., Marini, A., Fuchs, S., 2018. Vulnerability to flash floods: a simplified structural model for masonry buildings. Water Resour. Res. 54. https://doi.org/10.1029/2018WR022577.

Molinari, D., Ballio, F., Handmer, J., Menoni, S., 2014. On the modeling of significance for flood damage assessment, 2014 Int. J. Disaster Risk Reduct. 10 (part A), 381–391. https://doi.org/10.1016/j.ijdrr.2014.10.009.

Molinari, D., Scorzini, A.R., Gallazzi, A., Ballio, F., 2019. AGRIDE-c, a conceptual model for the estimation of flood damage to crops: development and implementation. Nat. Hazards Earth Syst. Sci. 19, 2565–2582. https://doi.org/10.5194/nhess-19-2565-2019.

Molinari, D., Scorzini, A.R., Arrighi, C., Carisi, F., Castelli, F., Domeneghetti, A., Gallazzi, A., Galliani, M., Grelot, F., Kellermann, P., Kreibich, H., Mohor, G.S., Mosimann, M., Natho, S., Richert, C., Schroeter, K., Thieken, A.H., Zischg, A.P., Ballio, F., 2020. Are flood damage models converging to "reality"? Lessons learnt from a blind test. Nat. Hazards Earth Syst. Sci. 20, 2997–3017. https://doi.org/10.5194/nhess-20-2997-2020, 2020.

Molinari, D., Dazzi, S., Gattai, E., et al., 2021. Cost–benefit analysis of flood mitigation measures: a case study employing high-performance hydraulic and damage modelling. Nat. Hazards 108, 3061–3084. https://doi.org/10.1007/s11069-021-04814-6.

Petaccia, G., Natale, L., 2020. 1935 Sella Zerbino dam break case revisited: a new Hydrologic and Hydraulic analysis,. J. Hydraul. Eng. 146 (8) https://doi.org/10.1061/(ASCE)HY.1943-7900.0001760.

Pilotti, M., Maranzoni, A., Tomirotti, M., Valerio, G., 2011. The 1923 Gleno dam-break: case study and numerical modelling. J. Hydraul. Eng., ASCE Volume 137, 480. https://doi.org/10.1061/(ASCE)HY.1943-7900.0000327.

Pilotti, M., Valerio, G., Leoni, B., 2013. Data set for hydrodynamic lake model calibration: a deep pre-alpine case. Water Resour. Res. 49, 7159–7163. https://doi.org/10.1002/wrcr.20506.

Pilotti, M., Farina, G., Bonomelli, R., Milanesi, L.. Physically Based Vulnerability Functions for flood risk mapping in mountain area. https://doi:10.3850/IAHR-39WC252171192022458.

Pregnolato, M., Galasso, C., & Parisi, F. 2015. A Compendium of Existing Vulnerability and Fragility Relationships for Flood: Preliminary Results, *Proceedings of the 12th International Conference on Applications of Statistics and Probability in Civil Engineering, ICASP12*, Vancouver, Canada, 12–15 July 2015, 397, https://doi.org/10.14288/1.0076226.

Simonelli, T., Zoppi, L., Molinari, D., Ballio, F., 2022. Invited perspectives: When research meets practice: challenges, opportunities, and suggestions from the implementation of the Floods Directive in the largest Italian river basin. Nat. Hazards Earth Syst. Sci. 22, 1819–1823. https://doi.org/10.5194/nhess-22-1819-2022.

Toro, E.F., 2001. Shock Capturing Methods for Free Surface Shallow Flows. Wiley and Sons.

Toro, E.F., 2009. Riemann Solvers and Numerical Methods for Fluid Dynamics: A Practical Introduction. Springer, Berlin, Heidelberg. https://doi.org/10.1007/b79761.

Van der Meulen, B., Cohen, K.M., Pierik, H.J., Zinsmeister, J.J., Middelkoop, H., 2020. LiDAR-derived high-resolution paleo-DEM construction workflow and application to the early medieval lower Rhine valley and upper delta. Geomorphology 370, 107370. https://doi.org/10.1016/j.geomorph.2020.107370.

Vázquez-Cendón, E., 2015. Solving Hyperbolic Equations with Finite Volume Methods. Springer Cham. https://doi.org/10.1007/978-3-319-14784-0.

Wei, Ge, Xiuwei, Wang, Zongkun, Li, Hexiang, Zhang, Guo, Xinyan, Wang, Te, Gao, Weixing, Lin, Chaoning, van Gelder, Pieter, 2021. Interval analysis of the loss of life caused by dam failure. J. Water Resour. Plan. Manag. 147, 1,https://doi.org/10.1061/(ASCE)WR.1943-5452.0001311.

Yoon, T., H, ASCE, F., Kang, S., K, 2004. Finite volume model for two-dimensional shallow water flows on unstructured grids. J. Hydraul. Eng. 130, 678–688. https://doi.org/10.1061/(ASCE)0733-9429(2004)130:7(678).